Fluorescent Probes

International Edition: DOI: 10.1002/anie.201907410
German Edition: DOI: 10.1002/ange.201907410

Direct Visualization of Live Zebrafish Glycans via Single-Step Metabolic Labeling with Fluorophore-Tagged Nucleotide Sugars

Senlian Hong[+], Pankaj Sahai-Hernandez[+], Digantkumar Gopaldas Chapla, Kelley W. Moremen, David Traver, and Peng Wu**

Abstract: *Dynamic turnover of cell-surface glycans is involved in a myriad of biological events, making this process an attractive target for in vivo molecular imaging. Metabolic glycan labeling coupled with bioorthogonal chemistry has paved the way for visualizing glycans in living organisms. However, a two-step labeling sequence is required, which suffers from the tissue-penetration difficulties of the imaging probes. Here, by exploring the substrate promiscuity of endogenous glycosyltransferases, we developed a single-step fluorescent glycan labeling strategy by using fluorophore-tagged analogues of the nucleotide sugars. Injecting fluorophore-tagged sialic acid and fucose into the yolk of zebrafish embryos at the one-cell stage enables systematic imaging of sialylation and fucosylation in live zebrafish embryos at distinct developmental stages. From these studies, we obtained insights into the role of sialylated and fucosylated glycans in zebrafish hematopoiesis.*

Introduction

Metabolic oligosaccharide engineering (MOE) coupled with the bioorthogonal chemical reporter strategy has opened an avenue for labeling and visualizing glycans in living organisms.[1–5] In this approach, the glycan biosynthetic machinery of the cell is exploited to install a biorthogonal chemical group onto cell-surface glycans, which is then covalently labeled in a secondary step with a complementary probe.[6] However, this strategy has a few intrinsic limitations, such as the biocompatibility of a chosen bioorthogonal reaction and poor deep-tissue penetration of the probes.[7]

Chemoenzymatic glycan editing, however, enables the direct incorporation of a fluorescently labeled monosaccharide without the requirement of a second-step. By using recombinant sialyltransferases (STs) and fucosyltransferases (FTs) with broad donor substrate scopes, sialic acid (Sia) and fucose (Fuc) conjugated with fluorescent dyes can be directly transferred to the cell surface from the corresponding nucleotide sugars.[8–11] Furthermore, recent findings have shown that fluorescently labeled trehalose and *N*-acetylglucosamine can be directly incorporated into the cell wall of *M. tuberculosis*[12] and intracellular *O*-GlcNAcylated proteins in cultured mammalian cells,[13] respectively. Inspired by these findings, here, we sought to explore the feasibility of directly incorporating fluorophore-labeled monosaccharides into the cellular glycans of living organisms by exploiting the substrate promiscuity of endogenous glycosyltransferases (Figure 1 a).

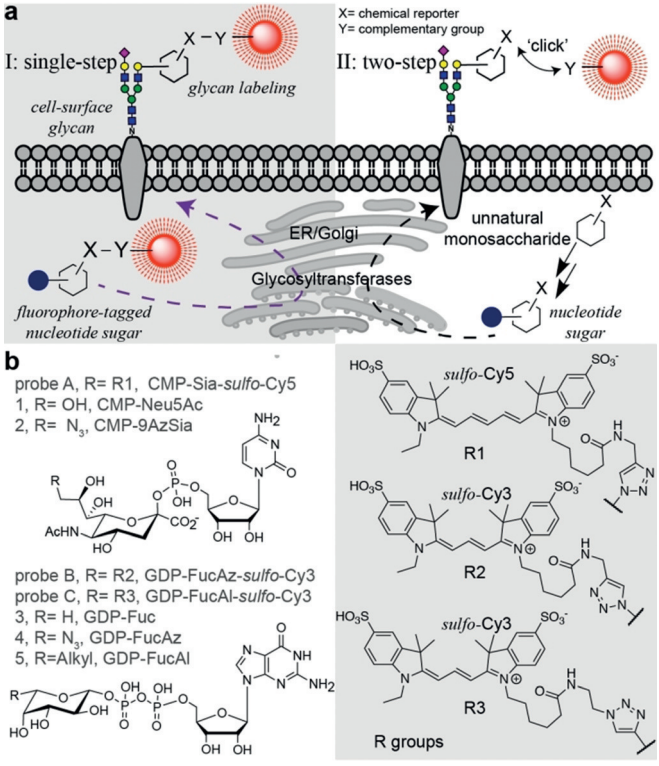

Figure 1. a) Comparison of the single-step fluorescent glycan visualization via the metabolic incorporation of unnatural fluorophore-tagged nucleotide sugars versus the conventional, two-step approach. b) Nucleotide sugar analogues functionalized with a chemical reporter (alkyl and azido) or a fluorophore (Cy3 and Cy5) that were used in this study.

[*] Dr. S. Hong,[+] Prof. P. Wu
Department of Molecular Medicine, The Scripps Research Institute
10550 North Torrey Pines Road, La Jolla, CA 92037 (USA)
E-mail: pengwu@scripps.edu
Dr. P. Sahai-Hernandez,[+] Prof. D. Traver
Department of Cellular and Molecular Medicine,
University of California at San Diego, La Jolla, CA 92037 (USA)
E-mail: dtraver@ucsd.edu
Dr. D. G. Chapla, Prof. K. W. Moremen
Complex Carbohydrate Research Center, University of Georgia
Athens, GA 30602 (USA)
[+] These authors contributed equally to this work.
Supporting information and the ORCID identification number(s) for the author(s) of this article can be found under: https://doi.org/10.1002/anie.201907410.

Results and Discussion

We assessed the incorporation of fluorophore-labeled monosaccharides in live zebrafish embryos due to their optical transparency, external fertilization, and amenability to genetic and embryological manipulations.[14–16] First, we synthesized a fluorophore-labeled CMP-*N*-acetylneuraminic acid (CMP-Neu5NAc). Previous studies have shown that many STs can tolerate large substituents at C9 of Neu5NAc.[17,18] Therefore, we synthesized CMP-Sia-sulfo-Cy5 (probe A) by coupling CMP-9AzSia[19] with Al-sulfo-Cy5 via ligand (BTTP)-assisted copper-catalyzed azide-alkyl [3+2] cycloaddition (CuAAC).[20]

To first validate that the Cy5-tagged CMP-Sia analogue can be incorporated by STs in live cells, we examined the feasibility of transferring Sia-sulfo-Cy5 onto the cell-surface of sialylation-deficient Lec2 mutant Chinese hamster ovary (CHO) cells, using three recombinant human STs (hST3Gal1, hST3Gal4, hST6Gal1).[21] ST6Gal1/2 and ST3Gal1/2/3/4/5 are evolutionarily conserved in human and zebrafish genomes and STs in both species share high homology,[22–24] therefore it is reasonable to use the human homologues to examine the donor substrate scope. After incubation with STs and probe A, we detected intense Cy5 fluorescence on Lec2 cells, but not in the cells treated without STs (Supporting Information, Figure s1). This confirms that the STs have the capability to incorporate probe A into cell-surface glycans for single-step glycan labeling.

Next, we microinjected probe A into the yolk sack of zebrafish embryos at the one-cell stage,[25] which enables the injected nucleotide sugar to disperse and incorporate into all daughter cells during early zebrafish embryogenesis (Figure 2a). The injected embryos were subsequently imaged

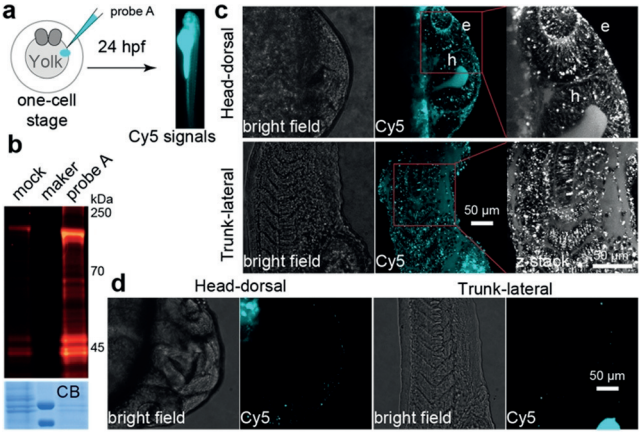

Figure 2. Metabolic incorporation of CMP-Sia-sulfo-Cy5 (probe A) onto sialylated glycan in live zebrafish embryos. a) Workflow of using probe A to fluorescently label sialylated glycan in zebrafish embryos. After a 24-hour incubation, the labeled glycoconjugates in live embryos were directly imaged. b) In-gel analysis of Cy5 fluorescence of labeled glycoproteins (top panel). The same counts of embryos were collected, deyolked, and the resulting lysate was loaded onto SDS-PAGE. The loading was evaluated by Coomassie-blue staining (CB). c,d) The confocal images of embryos injected with probe A (c), or prequenched reaction mixture (d, mock control). Intensive Cy5 fluorescence was detected in the eye (e) and hindbrain (h) regions of the head, in the somatic tissue, muscle cells, and intro-hypochord of the trunk.

using fluorescent microscopy at distinct developmental stages. As shown in Figure S2 in the Supporting Information, overwhelming fluorescent signals in the yolk due to the accumulation of probe A prevented the visualization of the incorporated Sia in other tissue structures during early embryogenesis. To our delight, the incorporation of probe A in several distinct tissue structures became apparent starting at 14 hours post fertilization (hpf). Importantly, the probe-dependent Cy5 signal in live embryos is significantly reduced by coinjection of the sialylation inhibitor 3FaxNeu5Ac[26] or the natural sialylation precursor CMP-Neu5Ac together with probe A (Supporting Information, Figure S3), suggesting specific labeling of sialylated glycans in zebrafish.

To confirm that probe A was metabolically incorporated into zebrafish glycoproteins, the lysates of the 24 hpf deyolked embryos were analyzed using an in-gel fluorescence assay. We detected strong probe A-dependent Cy5 signal in SDS-PAGE resolved proteins with molecular weights ranging from 30–250 kDa (Figure 2b and Supporting Information, Figure S4), which was largely abolished by PNGase F treatment to remove N-glycans from glycoproteins or neuraminidase treatment to remove Sia from glycoproteins (Supporting Information, Figure S5). Together, these results strongly suggest that CMP-Sia-sulfo-Cy5 is metabolically incorporated in sialylated glycoproteins.

Once we confirmed the specific labeling of probe A into the cell-surface glycoproteins, we proceeded to perform systematic imaging of sialylation in zebrafish tissues at 24 hpf. We observed distinct Cy5 fluorescence in the head and trunk regions (Figure 2c and Supporting Information, Movies S1 and S2). Specifically, in the eye and hindbrain regions of the brain, the hypochord in the trunk, and muscle cells in the somites exhibited strong Cy5 fluorescence. Importantly, in the control embryos that were injected with CMP-9AzSia and Al-sulfo-Cy5, only negligible background Cy5 signals was detected (Figure 2d). These observations are consistent with previous reports from Bertozzi and co-workers,[17,18] in which BCNSia was used as the metabolic substrate and the detection was realized by the reaction with a fluorogenic tetrazine probe injected into the posterior caudal vein. In this approach, imaging can only begin at 30 hpf, which is the earliest time at which the caudal vein starts to form. Since the incorporation of unnatural analogues onto glycans could potentially interfere with their biological functions, we further analyzed the morphological defects of zebrafish embryos injected with different concentrations of probe A (2.5, 5, or 10 pmol). At 24 hpf we did not observe any apparent morphological defects in any of the injected embryos (Supporting Information, Figure S6), suggesting that probe A does not interfere with normal biological functions.

Next, we expanded this design to directly probe another type of glycosylation known as fucosylation. We prepared a Cy3-tagged GDP-Fuc analogue by conjugating the GDP-FucAz[27] with Al-sulfo-Cy3 (Supporting Information, Figure S7b). However, embryos injected with GDP-FucAz-sulfo-Cy3 (probe B) exhibited gross morphological defects including bent tails and twisted notochords. Furthermore, defects increased in severity as concentration of probe B increased (Supporting Information, Figure S8). This pheno-

type was also observed in the GDP-FucAz-injected group, and in embryos injected with a mixture of GDP-FucAz and Al-sulfo-Cy3. As an alternative, we chose to use GDP-6-alkylfucose (GDP-FucAl), which has better biocompatibility, to prepare a Cy3-tagged analogue (GDP-Fuc-sulfo-Cy3, Supporting Information, Figure S7a).[28] To our delight, embryos treated with GDP-Fuc-sulfo-Cy3 (probe C) exhibited no apparent morphological defects compared to the natural GDP-Fuc-treated group.

To image fucosylated glycans in live zebrafish embryos, we injected the sulfo-Cy3-bearing probe B and probe C into the yolk of one-cell stage embryos and performed confocal imaging of the embryos at 24 hpf (Supporting Information, Movies S3 and S4). Embryos injected with both probes showed intense Cy3 fluorescence in the brain and trunk regions without any observable differences in labeling patterns. By contrast, control group embryos showed no specific labeling except for dye trapped within the yolk region. Importantly, probe C-dependent Cy3-labeling was suppressed when probe C was coinjected with fucosylation inhibitor 2-fluoro-fucose[26] or the natural donor GDP-Fuc (Supporting Information, Figure S9). Furthermore, the Cy3-associated fluorescence in the embryo-lysate was significantly abolished after PNGase F treatment (Supporting Information, Figure S10). These results strongly suggest that GDP-Fuc-sulfo-Cy3 is metabolically incorporated into zebrafish fucosylated glycans. Similar to our observation for recombinant human STs, recombinant human FTs, including hFuT6, hFuT7, and hFuT9, were also capable of adding Cy3-tagged Fuc onto Lec2 glycans using probe C as a substrate. In labeled-Lec2 cells, we imaged robust Cy3 labeling compared to the cells treated without hFuTs (Supporting Information, Figure s11).

Due to the toxicity of probe B, systematic imaging of fucosylation was conducted with probe C, even though probe C showed weaker incorporation. Confocal images of live zebrafish embryos injected with probe C at 24 hpf revealed a highly localized distribution of labeled fucosides in the head (lateral, ventral, and dorsal views) and trunk regions (lateral view, Figure 3 and Supporting Information, Figure S11 and Movies S5 and S6). Abundant fucosylation was specifically detected within the eye, olfactory placode, midbrain, hindbrain, hypochord, dorsal fin, blood vessels, and the caudal hematopoietic tissue (cht). The incorporation appeared more intense in neural structures, such as the midbrain and the hindbrain. Interestingly, the midbrain–hindbrain boundary (mhb) did not show any incorporation of the unnatural fucose. Moreover, this strategy also enabled time-lapse tracking of fucosylated glycans in live zebrafish embryos. For example, Cy3-labeled fucoside was abundant in the retina and the optical cup of the eyes, and moved dynamically along the ganglia of acetylated microtubules, which are regarded as stable, long-lived microtubules[48] (Time points 4-t1 and 4-t2 in Figure 3b and Supporting Information, Movie S7).

The ability to simultaneously visualize distinct biomolecules in vivo is of essential importance for understanding normal and disease processes. We then evaluated the feasibility of visualizing sialylated and fucosylated glycans in

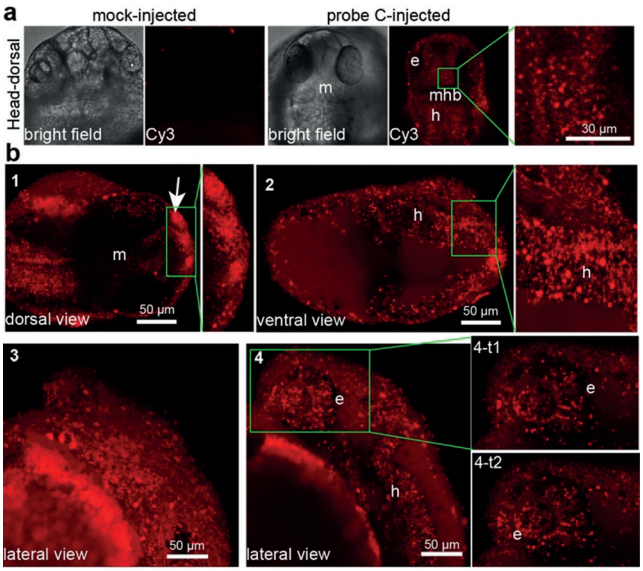

Figure 3. Systematic visualization of fucosylation in live zebrafish by metabolic incorporation of GDP-FucAl-sulfo-Cy3 (probe C) onto fucosylated glycans. a) confocal images of embryos injected with probe C or prequenched reaction mixture (mock control). In probe C-injected embryos, strong Cy3 fluorescence was detected in the eye (e), midbrain (m), and hindbrain (h) regions, while only negligible background fluorescence was detected at the midbrain–hindbrain boundary (mhb) as shown in the high magnification image of the dorsal view of the midbrain. b) Dorsal view (1 and 2) of a head at different depths, the developing mouth showed intensive fucosylation (arrow). Lateral views of the head surface (3) and in deep-tissue at different time points (4, 4-t1, and 4-t2).

parallel. To this end, we co-injected probe A and probe C at a 1:1 molar ratio into the yolk of zebrafish embryos and conducted confocal imaging at different time points (Figure 4a and Supporting Information, Figure S12). As shown in Figure 4a, sialylated glycans have broader distributions than their fucosylated counterparts at 24 hpf embryos. The blood vessels showed the strongest co-localization of both glycans. However, these two types of glycans also exhibited many distinct distribution patterns. For example, sialylation was abundantly detected in the notochord and myotome region, while fucosylation was generally localized in the vascular network. Furthermore, the labeled fucoside decayed at a much faster rate than the labeled sialosides; by 72 hpf, the Cy3-associated signal disappeared almost completely in the brain; whereas abundant Cy5 signal was still detectable at this time (Supporting Information, Figure S13).

Next, we directly compared the labeling patterns of the single-step glycan labeling to the well-established two-step labeling strategy. We co-injected probe C and GDP-FucAz into the same embryo, and the metabolically incorporated FucAz was fluorescently labeled with Al-sulfo-Cy5 by BTTPS-assisted CuAAC reaction at 24 hpf. In deep tissues, such as the cht region, we only observed the Cy3 signal but not that of Cy5. Likewise, only a very weak Cy5 signal was detected in the trunk and head regions, which is likely due to the poor permeability of labeling reagents into the deep-tissue of live zebrafish embryos. The observation that a much stronger Cy5 signal was detected at the tip of the tail

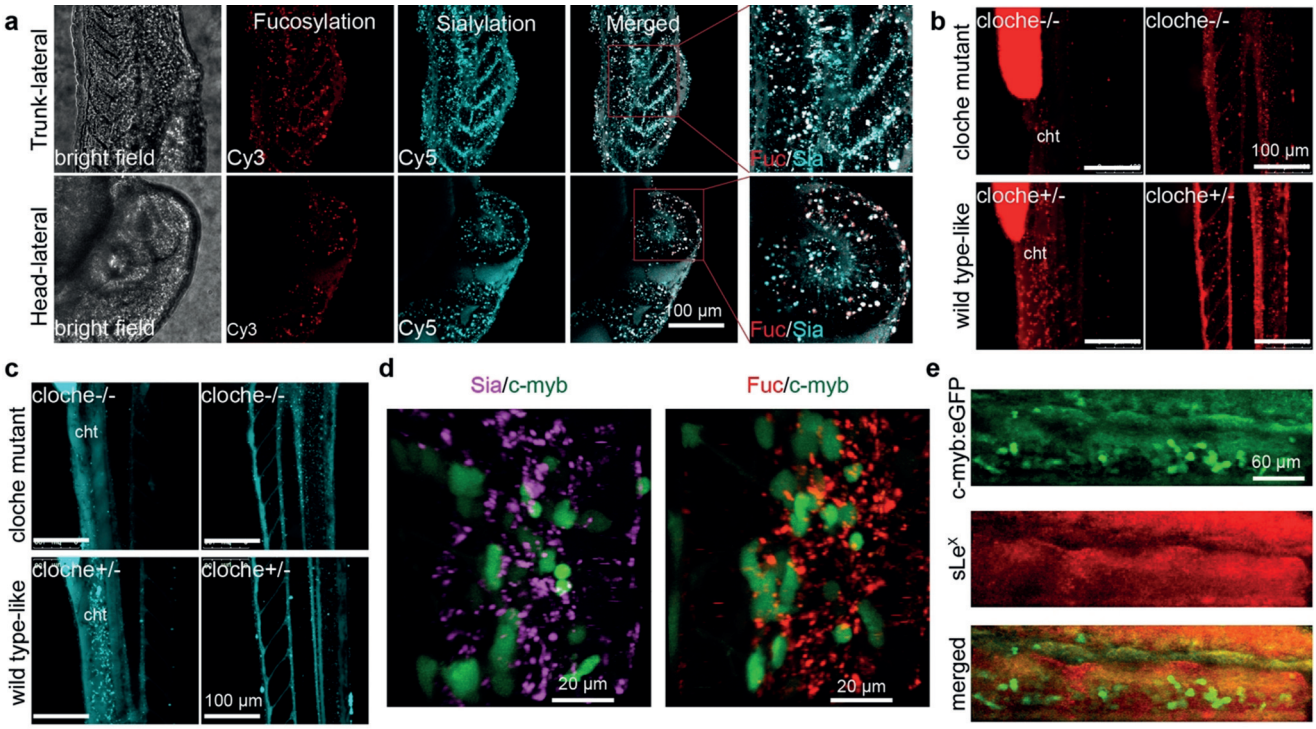

Figure 4. Simultaneous visualization of the deep-tissue fucosylation (Cy3 in red channel) and sialylation (Cy5 in cyan channel). a) The lateral view of zebrafish embryos co-injected with probe A and probe C at 24 hpf. b,c) The trunk (lateral view) of cloche mutant (cloche −/−) or wildtype-like siblings (cloche +/−) at 48 hpf was visualized at different depths. The fluorescence in the yolk served as an internal control for the success of microinjections. d) In the cht region of Tg(c-Myb:eGFP) embryos, HSCs (green channel) do not co-localize with the labeled fucosides and sialosides. e) In Tg(c-Myb:eGFP) embryos, HSCs do not co-localize with cells expressing sLe^X (red) in the cht region.

compared to the Cy3 signal is likely caused by the same issue (Supporting Information, Figure S14). Similar results were also observed in zebrafish embryos coinjected with probe C and GDP-FucAl (Supporting Information, Figure S15).

To exclude the possibility that the observed labeling patterns were generated by unincorporated probes circling in the blood or diffusing into the tissue matrix, a hematopoietic mutant line known as cloche[29] was used to repeat our labeling experiments. In this mutant (cloche−/−), no vasculature, including the cht, is formed due to the failure to specify all blood-cell types in the developing embryos. We injected embryos from cloche mutant heterozygous (cloche +/−) parents with probe A or C. A distinct labeling pattern was detected in the trunk and head regions of wildtype-like sibling embryos (cloche +/−) that have normal hematovascular cell types, as we had previously observed. In the cloche−/− embryos that are easily distinguished by the lack of blood flow after 26 hpf, the loss of labeling was observed in tissues, such as the same region of the cht, due to the loss of vascular development (Figure 4b,c and Supporting Information, Movie S8–S11). Based on these observations, we reasoned that the background fluorescence generated by the free, unincorporated probes in the bloodstream is negligible.

The cht region is a transient vascular network formed by the ramification of the caudal vein plexus and provides a necessary niche microenvironment for supporting the development of nascent hematopoietic stem cells (HSCs).[30] The cht is of critical importance for the maturation of these blood-cell and immune-cell types. To explore the possible biological functions of glycans within this compartment, we imaged probe A- and probe C-injected zebrafish expressing the hematopoietic marker Tg(cMyb:eGFP),[31] which enables the tracking of the HSCs produced by definitive hematopoiesis (Figure 4d and Supporting Information, Movie S12, and S13). Definitive hematopoiesis produces multi-potent blood-cell types that give rise to multiple lineages through cellular intermediates and supports the production of all blood cells throughout adulthood. Within the cht region, we observed that the fluorescently labeled sialosides and fucoside were present in cells that are in direct contact with the eGFP-expressing HSCs, but not within the HSCs themselves. Previous studies have reported that sialyl-Lewis X (sLe^X, Siaα2-3Galβ1-4(Fucα1-3)-GlcNAc) plays critical roles in mediating leukocyte adhesion and lymphocyte homing,[32,33] we immunostained sLe^X epitopes in Tg(c-Myb:eGFP)-expressing embryos with an anti-cutaneous lymphocyte-associated antigen (CLA) antibody (Figure 4d). Despite the high fluorescence background, the intensive staining within the cht region was predominantly found in the extracellular matrix, rather than co-localizing with HSCs. This observation strongly suggests that the interactions mediated by sialylated and fucosylated glycans, such as sLe^X, are involved in the hematovascular cell biology in zebrafish.

During these imaging studies, we made an intriguing observation: compared to their sibling embryos (cloche +/−), the incorporation of GDP-Fuc-based probe C was significantly decreased in the mutant embryos (cloche−/−); whereas the incorporation of CMP-Sia-based probe A was essen-

tially unchanged (Figure 4b,c). Interestingly, compared to the untreated or the probe A-injected groups approximately 5-fold more cloche−/− mutant embryos were still alive at 48 hpf in the probe C-injected group (Supporting Information, Figure S16a). These observations prompted us to examine the expression of fucoside biosynthesis enzymes in the cloche mutants. We performed RT-qPCR analysis of gene expression of key components of the GDP-Fuc de novo biosynthesis and salvage pathways (Supporting Information, Figure S17a), and found that the mRNA levels of fucose kinase (FUK) and GDP-Fuc transporter (SLC35C1) were significantly down-regulated in the cloche−/− mutants (Supporting Information, Figure s17b). Consistent with those changes, the global fucosylation in cloche−/− embryos was significantly decreased compared to that of the wildtype embryos or their siblings (cloche+/−) as assessed by fluorescein-conjugated *Aleuria Aurantia* Lectin (AAL-FITC) staining (AAL is a lectin specific for α1-3- and α1-6-linked fucose, Figure 5a). By administering GDP-Fuc into embryos of the cloche−/− mutants at the one-cell stage, the global fucosylation level were largely rescued (Figure 5b).

All vertebrates, including zebrafish, have two waves of hematopoiesis[34,35] The earlier of these is known as the primitive wave and the later one as the definitive wave. The primitive wave is responsible for the production of red blood cell types that can facilitate tissue oxygenation as the embryo undergoes rapid growth; whereas definitive or adult hematopoiesis provides the organism with long-term HSCs that are capable of unlimited self-renewal and generating all mature hematopoietic lineages. The cloche−/− mutant exhibits serious defects in both waves, but interestingly the absence of vascular cells is partially rescued by 48 hpf.[29]

To decipher the role that fucosylation might play during early zebrafish hematopoietic development, we injected Fuc or GDP-Fuc into transgenic zebrafish lines harboring reporters of hematopoiesis and followed their development. Although no convincing findings were made using reporter lines of the primitive wave, in the transgenic zebrafish line Tg(cMyb:eGFP), whose definitive blood progenitors can be directly traced by eGFP-expression, Fuc and GDP-Fuc injection distinctively increased the population of eGFP-labeled HSCs in the cht niche region between 48–72 hpf. These changes were not detectable in mock and CMP-Neu5Ac-treated groups (Figure 5c,d). Finally, we also identified significantly larger number of live cloche−/− mutant embryos 48 hpf after the administration of Fuc or GDP-Fuc compared to CMP-Neu5Ac-treated or mock-treated groups (Supporting Information, Figure S16b).

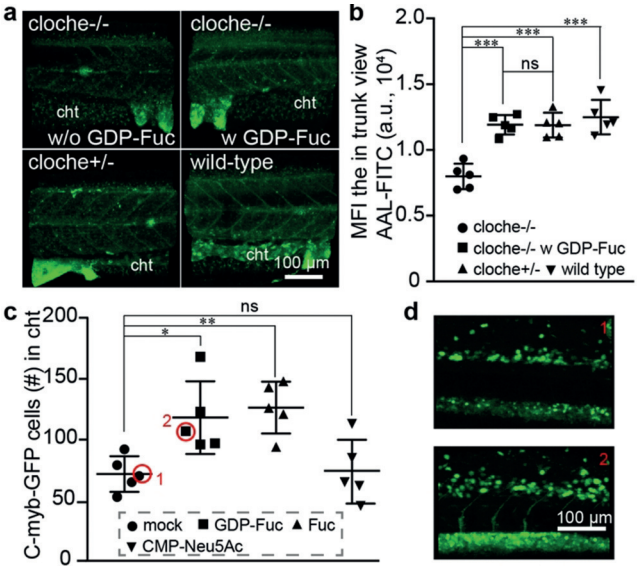

Figure 5. Impaired global fucosylation was observed in the cloche mutant (cloche−/−). a) The 3D confocal images of the fucosylation in the trunk of different embryos that were stained by AAL-FITC. The wildtype, cloche mutant (cloche−/−), wildtype-like sibling (cloche+/−), and GDP-Fuc-injected cloche mutant were collected at 48 hpf and stained with AAL-FITC after fixation and permeabilization. b) The fluorescent intensity in the trunk view of embryos was quantified and presented using the mean fluorescence intensity (MFI) via ImageJ. c,d) Confocal imaging-assisted counting of HSCs cells in the cht. Tg(c-Myb:eGFP) embryos at the 1–2 cell stage were injected with Fuc, GDP-Fuc, CMP-Neu5Ac, or mock loading buffer, and the HSCs were quantified at 48 hpf. The * represents $p<0.05$, the ** represents $p<0.01$, the *** represents $p<0.001$ and the ns represents not significant in the T-test.

Conclusion

Previous studies by Bertozzi and by us demonstrated that unnatural UDP-GalNAc bearing an azide tag and GDP-fucose bearing an azide or alkyne tag can be used by endogenous ppGalNActransferases and fucosyltransferases, respectively, and incorporated into cellular glycoconjugates in zebrafish embryos.[27,36,49] Bioorthogonal chemistry can then be employed for their visualization as early as at the two-cell stage. Via this approach, rapid glycan migration to the cleavage furrow of mitotic cells was observed despite poor tissue penetration of fluorescent probes used for their detection.

In the current study, we have demonstrated that fluorophore-tagged CMP-sialic acid and GDP-fucose (probes A–C) injected into the yolk of zebrafish embryos are incorporated onto cellular glycoconjugates, enabling the direct deep-tissue visualization of sialylated and fucosylated glycans. Using this single-step approach, time-lapse, high-resolution confocal imaging of these biologically important glycans in zebrafish embryogenesis is realized. Importantly, this approach enables the direct visualization of the dynamic turnover of glycans in live embryos. For example, we observed that in the head region, fucosylated glycans have a quicker turnover rate than sialylated glycans.[24,37,38]

Studies by Stanley, Haltiwanger, and Taniguchi have shown that knockout of the fucosyltransferases FUT8, POFUT1, or POFUT2 is lethal to mice.[39–42] Furthermore, congenital mutations of the Golgi-localized GDP-fucose transporter SLC35C1 cause leukocyte adhesion deficiency type II, which manifests as severe developmental and immune deficiencies.[43] In line with these previous observations, we discovered that the cloche mutation leads to down-regulation of *fuk* and *slc35c1,* and accordingly reduced cell-surface fucosylation, which can be partially compensated by exoge-

nously introduced Fuc or GDP-Fuc. Interestingly, not only did Fuc or GDP-Fuc injection expand the HSC population in the cht niche, but this treatment also increased the survival of the early-stage cloche mutant significantly (less than 48 hpf). Our findings combined with previous reports[44–47] underscore the critical role of fucosylation in hematopoiesis, especially in the definitive wave, though the exact molecular mechanism for our observed phenotypes is still waiting to be further explored.

Acknowledgements

Financial support was from the NIH (R01GM113046, R01GM111938, and R01GM093282 to P.W., P41GM103390, P01GM107012, and R01GM130915 to K.W.M., R01DK074482 to D.T.).

Conflict of interest

The authors declare no conflict of interest.

Keywords: fluorophore-tagged nucleotide sugar · fucosylation · glycan labeling · fluorescent probes · sialic acids

How to cite: *Angew. Chem. Int. Ed.* **2019**, *58*, 14327–14333
Angew. Chem. **2019**, *131*, 14465–14471

[1] O. T. Keppler, R. Horstkorte, M. Pawlita, S. W. Reutter, *Glycobiology* **2001**, *11*, 11R—18R.
[2] S. T. Laughlin, J. M. Baskin, S. L. Amacher, C. R. Bertozzi, *Science* **2008**, *320*, 664–667.
[3] S. T. Laughlin, C. R. Bertozzi, *Proc. Natl. Acad. Sci. USA* **2009**, *106*, 12–17.
[4] R. Xie, L. Dong, R. Huang, S. Hong, R. Lei, X. Chen, *Angew. Chem. Int. Ed.* **2014**, *53*, 14082–14086; *Angew. Chem.* **2014**, *126*, 14306–14310.
[5] K. Kang, S. Joo, J. Y. Choi, S. Geum, S. P. Hong, S. Y. Lee, Y. H. Kim, S. M. Kim, M. H. Yoon, Y. Nam, et al., *Proc. Natl. Acad. Sci. USA* **2015**, *112*, E241–E248.
[6] J. A. Prescher, C. R. Bertozzi, *Nat. Chem. Biol.* **2005**, *1*, 13–21.
[7] C. R. Bertozzi, *Acc. Chem. Res.* **2011**, *44*, 651–653.
[8] C. J. Capicciotti, C. Zong, M. O. Sheikh, T. Sun, L. Wells, G. J. Boons, *J. Am. Chem. Soc.* **2017**, *139*, 13342–13348.
[9] L. Wen, D. Liu, Y. Zhang, K. Huang, X. Cao, J. Song, P. G. Wang, *ACS Cent. Sci.* **2018**, *4*, 451–457.
[10] J. Li, M. Chen, Z. Liu, L. Zhang, B. H. Felding, K. W. Moremen, G. Lauvau, M. Abadier, K. Ley, P. Wu, *ACS Cent. Sci.* **2018**, *4*, 1633–1641.
[11] S. Hong, Y. Shi, N. C. Wu, G. Grande, L. Douthit, H. Wang, W. Zhou, K. B. Sharpless, I. A. Wilson, J. Xie, et al., *Nat. Commun.* **2019**, *10*, 1799.
[12] K. M. Backus, H. I. Boshoff, C. S. Barry, O. Boutureira, M. K. Patel, F. D'Hooge, S. S. Lee, L. E. Via, K. Tahlan, C. E. Barry, et al., *Nat. Chem. Biol.* **2011**, *7*, 228–235.
[13] H. Y. Tan, R. Eskandari, D. Shen, Y. Zhu, T. W. Liu, L. I. Willems, M. G. Alteen, Z. Madden, D. J. Vocadlo, *J. Am. Chem. Soc.* **2018**, *140*, 15300–15308.
[14] L. I. Zon, R. T. Peterson, *Nat. Rev. Drug Discovery* **2005**, *4*, 35–44.
[15] G. J. Lieschke, P. D. Currie, *Nat. Rev. Genet.* **2007**, *8*, 353–367.
[16] R. White, K. Rose, L. Zon, *Nat. Rev. Cancer* **2013**, *13*, 624–636.
[17] T. N. C. Ramya, E. Weerapana, L. Liao, Y. Zeng, H. Tateno, L. Liao, J. R. Yates, B. F. Cravatt, J. C. Paulson, *Mol. Cell. Proteomics* **2010**, *9*, 1339–1351.
[18] P. Agarwal, B. J. Beahm, P. Shieh, C. R. Bertozzi, *Angew. Chem. Int. Ed.* **2015**, *54*, 11504–11510; *Angew. Chem.* **2015**, *127*, 11666–11672.
[19] S. Han, B. E. Collins, P. Bengtson, J. C. Paulson, *Nat. Chem. Biol.* **2005**, *1*, 93–97.
[20] W. Wang, S. Hong, A. Tran, H. Jiang, R. Triano, Y. Liu, X. Chen, P. Wu, *Chem. Asian J.* **2011**, *6*, 2796–2802.
[21] S. J. North, H. H. Huang, S. Sundaram, J. Jang-Lee, A. T. Etienne, A. Trollope, S. Chalabi, A. Dell, P. Stanley, S. M. Haslam, *J. Biol. Chem.* **2010**, *285*, 5759–5775.
[22] D. Petit, E. Teppa, A. M. Mir, D. Vicogne, C. Thisse, B. Thisse, C. Filloux, A. Harduin-Lepers, *Mol. Biol. Evol.* **2015**, *32*, 906–927.
[23] R. E. Teppa, D. Petit, O. Plechakova, V. Cogez, A. Harduin-Lepers, *Int. J. Mol. Sci.* **2016**, *17*, 1286.
[24] L. Y. Chang, E. Teppa, M. Noel, P. A. Gilormini, M. Decloquement, C. Lion, C. Biot, A. M. Mir, V. Cogez, P. Delannoy, et al., *Int. J. Mol. Sci.* **2019**, *20*, 622.
[25] C. B. Kimmel, R. D. Law, *Dev. Biol.* **1985**, *108*, 78–85.
[26] C. D. Rillahan, A. Antonopoulos, C. T. Lefort, R. Sonon, P. Azadi, K. Ley, A. Dell, S. M. Haslam, J. C. Paulson, *Nat. Chem. Biol.* **2012**, *8*, 661–668.
[27] K. W. Dehnert, B. J. Beahm, T. T. Huynh, J. M. Baskin, S. T. Laughlin, W. Wang, P. Wu, S. L. Amacher, C. R. Bertozzi, *ACS Chem. Biol.* **2011**, *6*, 547–552.
[28] D. S. del Amo, W. Wang, H. Jiang, C. Besanceney, A. C. Yan, M. Levy, Y. Liu, F. L. Marlow, P. Wu, *J. Am. Chem. Soc.* **2010**, *132*, 16893–16899.
[29] S. Reischauer, O. A. Stone, A. Villasenor, N. Chi, S. W. Jin, M. Martin, M. T. Lee, N. Fukuda, M. Marass, A. Witty, et al., *Nature* **2016**, *535*, 294–298.
[30] A. V. Gore, L. M. Pillay, M. Venero Galanternik, B. M. Weinstein, *Wiley Interdiscip. Rev. Dev. Biol.* **2018**, *7*, e312.
[31] J. Y. Bertrand, N. C. Chi, B. Santoso, S. Teng, D. Y. R. Stainier, D. Traver, *Nature* **2010**, *464*, 108–111.
[32] C. Foxall, S. R. Watson, D. Dowbenko, C. Fennie, L. A. Lasky, M. Kiso, A. Hasegawa, D. Asa, B. K. Brandley, *J. Cell Biol.* **1992**, *117*, 895–902.
[33] T. A. Springer, *Cell* **1994**, *76*, 301–314.
[34] A. J. Davidson, L. I. Zon, *Oncogene* **2004**, *23*, 7233–7246.
[35] W. K. Clements, D. Traver, *Nat. Rev. Immunol.* **2013**, *13*, 336–348.
[36] J. M. Baskin, K. W. Dehnert, S. T. Laughlin, S. L. Amacher, C. R. Bertozzi, *Proc. Natl. Acad. Sci. USA* **2010**, *107*, 10360–10365.
[37] M. Bardor, D. H. Nguyen, S. Diaz, A. Varki, *J. Biol. Chem.* **2005**, *280*, 4228–4237.
[38] P.-A. Gilormini, C. Lion, D. Vicogne, Y. Guérardel, F. Foulquier, C. Biot, *J. Inherited Metab. Dis.* **2018**, *41*, 515–523.
[39] S. Shi, P. Stanley, *Proc. Natl. Acad. Sci. USA* **2003**, *100*, 5234–5239.
[40] Y. Luo, K. Koles, W. Vorndam, R. S. Haltiwanger, V. M. Panin, *J. Biol. Chem.* **2006**, *281*, 9393–9399.
[41] X. Wang, S. Inoue, J. Gu, E. Miyoshi, K. Noda, W. Li, Y. Mizuno-Horikawa, M. Nakano, M. Asahi, M. Takahashi, et al., *Proc. Natl. Acad. Sci. USA* **2005**, *102*, 15791–15796.
[42] M. Schneider, E. Al-Shareffi, R. S. Haltiwanger, *Glycobiology* **2017**, *27*, 601–618.
[43] C. C. Hellbusch, M. Sperandio, D. Frommhold, S. Yakubenia, M. K. Wild, D. Popovici, D. Vestweber, H.-J. Gröne, K. von Figura, T. Lübke, et al., *J. Biol. Chem.* **2007**, *282*, 10762–10772.
[44] L. Zhou, L. W. Li, Q. Yan, B. Petryniak, Y. Man, C. Su, J. Shim, S. Chervin, J. B. Lowe, *Blood* **2008**, *112*, 308–319.

[45] L. Xia, J. M. McDaniel, T. Yago, A. Doeden, R. P. McEver, *Blood* **2004**, *104*, 3091 – 3096.
[46] A. Bigas, A. Robert-Moreno, L. Espinosa, *Int. J. Dev. Biol.* **2010**, *54*, 1175 – 1188.
[47] J. Myers, Y. Huang, L. Wei, Q. Yan, A. Huang, L. Zhou, *Transfusion* **2010**, *50*, 2660 – 2669.
[48] C. Janke, G. Montagnac, *Curr Biol* **2017**, *27*, R1287—R1292.
[49] H. Jiang, T. Zheng, A. López-Aguilar, L. Feng, F. Kopp, F. L. Marlow, P. Wu, *Bioconjug. Chem.* **2014**, *25*, 698 – 706.

Manuscript received: June 14, 2019
Accepted manuscript online: July 11, 2019
Version of record online: August 23, 2019

